Check for updates

Electrocatalysis

How to cite:
International Edition: doi.org/10.1002/anie.202209839
German Edition: doi.org/10.1002/ange.202209839

Nickel-Catalyzed Urea Electrolysis: From Nitrite and Cyanate as Major Products to Nitrogen Evolution

*Stephen W. Tatarchuk[+], Jury J. Medvedev[+], Feng Li, Yulia Tobolovskaya, and Anna Klinkova**

Abstract: The electrochemical urea oxidation reaction (UOR) to N_2 represents an efficient route to simultaneous nitrogen removal from N-enriched waste and production of renewable fuels at the cathode. However, the overoxidation of urea to NO_x^- usually dominates over its oxidation to N_2 at $Ni(OH)_2$-based anodes. Furthermore, detailed reaction mechanisms of UOR remain unclear, hindering the rational catalyst design. We found that UOR to NO_x^- on $Ni(OH)_2$ is accompanied by the formation of near stoichiometric amount of cyanate (NCO^-), which enabled the elucidation of UOR mechanisms. Based on our experimental and computational findings, we show that the formation of NO_x^- and N_2 follows two distinct vacancy-dependent pathways. We also demonstrate that the reaction selectivity can be steered towards N_2 formation by altering the composition of the catalyst, e.g., doping the catalyst with copper ($Ni_{0.8}Cu_{0.2}(OH)_2$) increases the faradaic efficiency of N_2 from 30 % to 55 %.

Introduction

Urea is an important industrial chemical that is widely used as a nitrogenous fertilizer and a raw material for the synthesis of formaldehyde resins, melamine, and barbiturates.[1] Urea is also used on a smaller scale in skincare products and for selective catalytic reduction of nitrogen oxides in flue gases.[1–3] As a result of its global use, a large amount of urea enters the environment with wastewaters from the urea production plants.[4,5] Additional urea contamination originates from mammalian protein metabolism and agricultural runoff.[4,5] In aquatic systems urea undergoes hydrolysis to ammonia, which causes algae blooms and further decomposes in air to hazardous nitrogen oxides.[6] Thus, urea waste treatment is essential to prevent its negative effects on the environment.[6,7]

[*] S. W. Tatarchuk,[+] Dr. J. J. Medvedev,[+] F. Li, Y. Tobolovskaya, Prof. A. Klinkova
Department of Chemistry and the Waterloo Institute for Nanotechnology, University of Waterloo
Ontario N2L 3G1 (Canada)
E-mail: aklinkova@uwaterloo.ca

[+] These authors contributed equally to this work.

The electrochemical urea oxidation reaction (UOR) to dinitrogen represents an environmentally friendly approach for the urea-enriched wastewater treatment, which enables simultaneous N removal and green hydrogen production.[4,9] The reactions taking place at the electrodes and the overall process are shown in equations 1–3. Due to a significant difference between the standard equilibrium potential of UOR and oxygen evolution reaction (OER): 0.07 V and 1.23 V vs RHE (reversible hydrogen electrode), respectively, theoretically ≈94 % less energy is required for the electrochemical production of H_2 through urea electrolysis than through water splitting (see Supporting Information, p. S4–S6).[9d] For the same reason, UOR to N_2 attracted attention as an alternative to OER reaction for electrochemical CO_2 utilization, and as a fuel for fuel cells.[9,10]

Cathode:

$$2H_2O + 2e^- \rightarrow H_2 + 2OH^- \quad (E^\circ = 0\ \text{V vs RHE}) \tag{1}$$

Anode:

$$CO(NH_2)_2 + 6OH^- \rightarrow N_2 + CO_2 + 5H_2O + 6e^- \quad (E^\circ = 0.07\ \text{V vs RHE}) \tag{2}$$

Overall:

$$CO(NH_2)_2 + H_2O \rightarrow N_2 + CO_2 + 3H_2 \quad (\Delta G^\circ = 39.5\ \text{kJ mol}^{-1};\ |E_{cell}{}^\circ| = 0.07\ \text{V}) \tag{3}$$

Over the past few decades, a lot of attention has been focused on the development and optimization of Ni-based catalysts for UOR due to their higher activity compared to noble metal-based catalysts (e.g., Pt, Rh, and Pt-Ir) and the abundance of Ni.[9] Different approaches were explored to improve the catalyst activity towards UOR, including doping with secondary metals (e.g., with Mo, Co, Fe, or Ru),[11] surface-chemistry engineering (e.g., incorporation of S or P),[12] or the introduction of defects or vacancies into the $Ni(OH)_2$ catalyst structure.[13] Despite significant progress in the field, the majority of the aforementioned works were focused exclusively on the UOR activity, while only a few of them discussed UOR products and factors affecting their selectivity.[13b,14] Moreover, it was usually assumed that UOR has 100 % N_2 selectivity, thus almost no attempts so far have been made to determine the structure-activity-selectivity relationships. Recently, Yang and co-workers demonstrated that urea electrolysis on an activated Ni foam (NF) anode

© 2022 Wiley-VCH GmbH

mainly led to the overoxidized products (e.g., NO_2^- and NO_3^-), while the faradaic efficiency (FE) of N_2 was poor (≈15 %).[13b] The authors showed that the FE of N_2 could be improved up to the record 30 % by modifying the anode surface with a polyaniline (PANI) layer, demonstrating the ability to steer product selectivity via surface engineering. However, detailed formation mechanisms of different products still remain unclear, hindering the rational design of UOR catalysts.

In this work, we focused on elucidating the mechanistic picture of UOR on the NiOOH surface by establishing the nature of the reaction by-products and systematically exploring the selectivity trends as a function of reaction parameters and the catalyst composition. To this end, we used nanostructured $Ni(OH)_2$ xerogel catalysts that have been previously shown to be highly active towards urea oxidation.[11d] The synthesized catalyst was deposited on a Ni foam support and electrochemically activated according to the method described in our previous work.[11d,15] A combination of in-line gas chromatography (GC), ion chromatography (IC), and nuclear magnetic resonance (NMR) was used for qualitative and quantitative product analysis. The disambiguated mechanistic pathways based on the experimental trends were further supported by density functional theory (DFT) calculations. The obtained mechanistic insights enabled us to devise a modified UOR catalyst with a record-breaking selectivity towards N_2.

Results and Discussion

First, to select meaningful potentials for potentiostatic electrolysis and product analysis, linear sweep voltammograms (LSVs) were recorded at $Ni(OH)_2$/NF in 1 M KOH in the absence and the presence of urea (Figure 1a). In the absence of urea, two waves were observed: the peak at 1.4–1.6 V vs RHE corresponding to $Ni^{2+} \rightarrow Ni^{3+}$ transition ($Ni(OH)_2$ to NiOOH) with an onset at $E = 1.37$ V vs RHE, which suggests that the dominate $Ni(OH)_2$ phase was β-$Ni(OH)_2$/β-NiOOH, and an onset at $E > 1.6$ V vs RHE corresponding to OER. In the presence of 0.33 M urea, catalytic currents of urea oxidation appeared at the Ni^{2+} oxidation potentials in agreement with previous reports.[9–14]

A series of short-term electrolyses at different anodic potentials (1.4–2.3 V) was performed to assess the influence of the applied potential on the product distribution (Figures 1b and S2). Ionic UOR products (NO_2^- and NO_3^-) were analyzed by IC and gas products were analyzed by GC (see details in Supporting Information, p. S2 and S3). The main products of UOR were nitrite, N_2 and nitrate (Figure 1b). Nitrite was the dominant product at all studied potentials with FE of up to 85 % at 1.7 V, while N_2 selectivity was generally poor (14–30 %). The highest FE of N_2 was observed at the very onset (30 % at 1.4 V), and the value decreased slightly with increasing potential (to ≈14 % at 2.3 V). In addition to nitrite and N_2, the formation of nitrate and oxygen were detected at $E > 1.7$ V. The FE of both products increased noticeably with increasing potential,

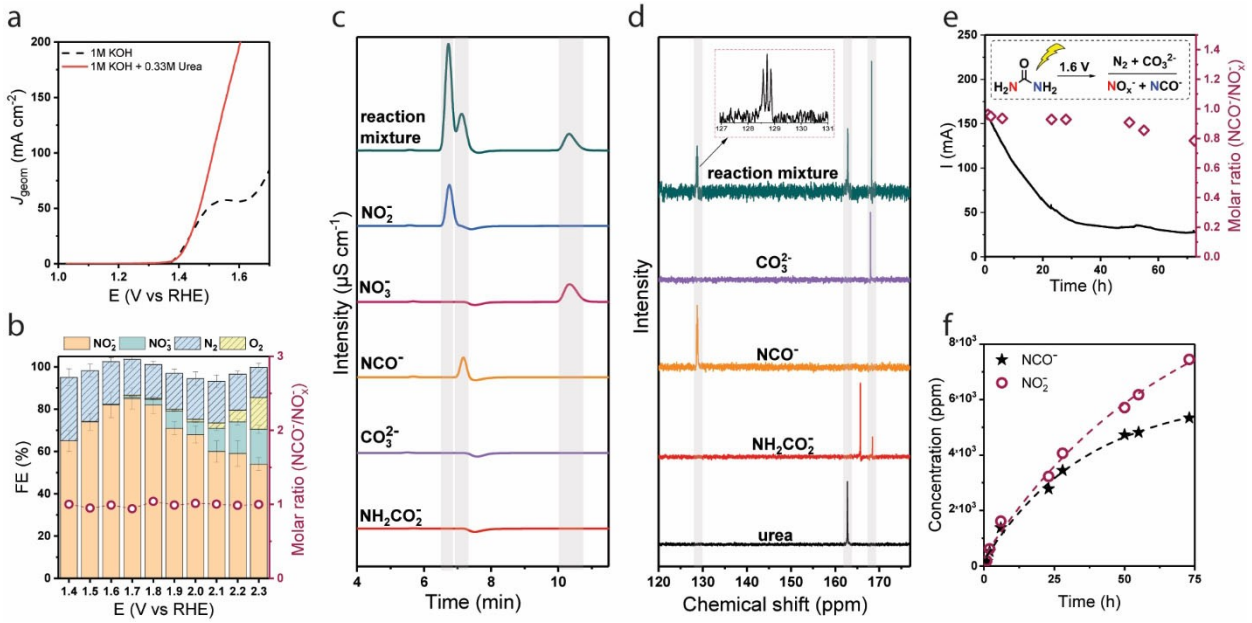

Figure 1. a) LSV curves recorded at 5 mV s^{-1} scan rate at the $Ni(OH)_2$/NF anode in 1 M KOH solution in the absence (dashed trace) and presence (solid trace) of 0.33 M urea. b) FEs of major products of short-term 1 h urea electrolysis and [NCO^-:NO_x^-] ($x = 1, 2$) molar ratio as a function of the applied potential. c) An example of the IC traces recorded for UOR reaction mixture compared to several standard anion solutions. d) An example of the NMR spectra recorded for long-term UOR at the $Ni(OH)_2$/NF anode compared to the NMR spectra of several carbon-containing anions and urea. e) A chronoamperometry curve was recorded for the preparative electrolysis of 0.33 M urea in 1 M KOH performed at 1.6 V and [NCO^-:NO_x^-] ($x = 1, 2$) molar ratio as a function of time. f) The concentrations of cyanate and nitrite in the electrolyte solution as a function of time in the preparative electrolysis of 0.33 M urea in 1 M KOH were performed at 1.6 V.

© 2022 Wiley-VCH GmbH

reaching the maximum at 2.3 V (17 % for nitrate and 15 % for O_2). We observed that the total FE of formed products deviated from 100 % under the studied potentials. To determine the minor products of urea electrolysis, we performed in-line gas chromatography mass spectroscopy (GC-MS) analysis of the reaction headspace at 1.5 V, 1.7 V and 1.9 V (Figures S3–S4). In addition to N_2 and O_2, we observed traces of N_2O and CO at all studied potentials with FEs of up to 1 % and 0.3 %, respectively (Figures S3 and S4).

Furthermore, the IC traces of all reaction mixtures contained an additional peak, revealing that UOR led to the formation of another anionic product in high quantities (Figure 1c). In a recent report, this additional IC peak was assigned to carbonate.[13b] However, the IC system used in the present work was equipped with a suppressor for the carbonate anion (see product analysis details in Supporting Information, p. S2–S3), indicating that another anion was produced in a course of electrolysis. To identify this unknown anion, its retention time in IC was compared to carbon-containing anions that could plausibly be produced from urea, specifically carbamate and cyanate (NCO^-). The retention time of the unknown anion matched that of NCO^-. Next, we analyzed the reaction mixtures using ^{13}C NMR to confirm the composition inferred from the IC data (Figure 1d). The NMR data showed that the reaction mixture consisted of three compounds containing a carbon atom, namely, urea, carbonate, and cyanate. The NCO^- signal in the ^{13}C NMR spectrum appeared as a triplet due to the scalar coupling of the adjacent ^{14}N nucleus, further confirming this assignment.[16]

In contrast to N_2, nitrite and nitrate, the oxidation states of all atoms in cyanate were the same as in urea. Thus, cyanate is not a product of direct electrochemical oxidation of the N and C in the urea molecule that became part of NCO^-, but rather a product of C–N bond cleavage during UOR. To prove that the applied potential is required for the formation of cyanate, we periodically performed the IC analysis of the urea solution in 1 M KOH over the course of three days, and no cyanate was detected (Figure S5). To assess which UOR pathway could be responsible for its formation, we compared the molar ratio of cyanate and other UOR products. Interestingly, at all potentials the concentration of cyanate formed in a course of electrolysis was nearly equal to the total concentration of NO_x^- products. This near-stoichiometric ratio suggested that the formation of cyanate was mechanistically associated with the NO_x^- pathway, while the N_2 pathway did not result in cyanate formation. We also performed preparative electrolysis of 0.33 M urea in 1 M KOH at an arbitrary potential (1.6 V) to determine how the concentration of nitrite and cyanate changed in the course of electrolysis (Figure 1e,f). The current decreased almost linearly during the first 20 h of electrolysis, which corresponded to the transfer of $\approx$2 mol of electrons per mol of urea. An exponential decay in the current was observed after 20 h, which then plateaued after 3.2 mol of electrons per mol of urea were transferred ($\approx$62 h). The changes in the solution composition during electrolysis were monitored using IC (Figure 1f). During the first several hours of electrolysis the molar ratio of cyanate and nitrite was close to 1:1, in agreement with the results of the short-term electrolysis described above. However, the NCO^-:NO_2^- ratio decreased with the urea depletion and reached 0.8:1 by the time the electrolysis was stopped, suggesting that cyanate itself can also undergo electrochemical oxidation. The total FE of nitrite at the end of electrolysis was 88 %, and the concentration of nitrite and cyanate was 0.16 M and 0.13 M, respectively.

The above results indicated that N_2 and the products of urea overoxidation originated from two independent reaction pathways, with the latter being accompanied by the formation of cyanate as a by-product in a stoichiometric amount to NO_x^-. In contrast, recent studies suggested carbamate ($NH_2CO_2^-$) as a by-product of UOR.[13b] To gain mechanistic insights into whether and how these compounds can participate in the UOR process, we compared the electrochemical behaviour of urea, carbamate, and cyanate with the same N concentration at $Ni(OH)_2$/NF anode (Figure S6). We found that among these compounds, urea has the highest activity followed by carbamate and cyanate with current densities ratio of $\approx$3.7:2.2:1, respectively. The potentiostatic electrolysis performed at 1.6 V showed very similar outcomes of UOR and cyanate oxidation with FE of nitrite of 80 %. This observation along with the poor kinetics of cyanate oxidation supports the hypothesis of a slow cyanate depletion during long-term UOR. The electrochemical oxidation of carbamate led to the formation of nitrite with FE of 98 %, and no formation of cyanate or N_2 was observed, indicating that carbamate cannot be an intermediate of either N_2 pathway or urea overoxidation pathway.

Considering the results obtained here and prior literature,[9–14] we rationalized plausible reaction mechanisms for the $NO_x^- + NCO^-$ pathway and $N_2 + CO_2$ pathway (with CO_2 turning into CO_3^{2-} in basic media), summarized in Figure 2. Since both N and C in cyanate maintain the same oxidation states as in urea, the $NO_x^- + NCO^-$ formation pathway requires only one N atom to be oxidized by the electrocatalyst surface (ultimately resulting in NO_x^-), while the second N atom does not require interaction with the surface and oxidation. The cleavage of the bond between this second nitrogen atom and the carbon atom in the urea molecule leads to the formation of NCO^- and its release into the bulk of the solution, while the *NH species remaining on the surface undergo further oxidation steps (Figure 2a). These subsequent oxidation steps are indistinguishable from the later steps of ammonia oxidation to nitrite and nitrate, which we recently described in detail.[15,17] We note that N_2 could also be formed through this pathway, however, the overoxidation pathways are more energetically favourable.[15,17]

In contrast to the $NO_x^- + NCO^-$ formation mechanism described above, N_2 formation results from both N centres in urea undergoing oxidation, which requires both of them to bind to the catalytic active sites enabling electron transfer from both N centres to the anode. To this end, a triangular intermediate with nitrogen-nitrogen-carbon heterocycle (diaziridine-3-one) was previously proposed, stemming from

© 2022 Wiley-VCH GmbH

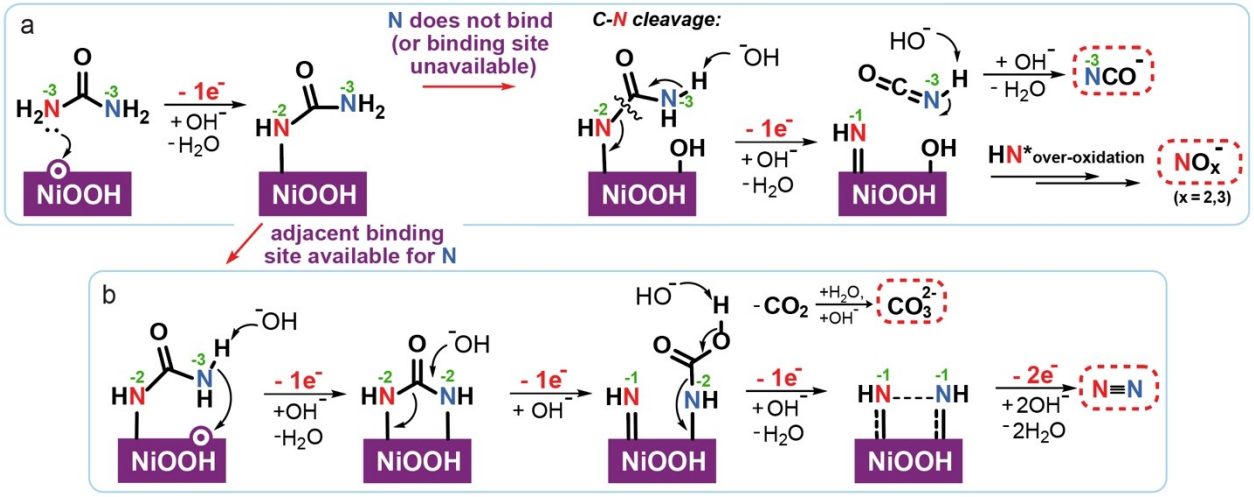

Figure 2. A schematic illustration of the proposed pathways for UOR to N_2 and CO_3^{2-} (a) and to NO_x^- and NCO^- (b) on the NiOOH surface (the green numbers above N atoms correspond to the nitrogen oxidation state).

the experimental evidence that both N atoms in N_2 predominantly originate from the same urea molecule.[13b,18] However, the same outcome can also be achieved when the C–N bond is cleaved, if the two nitrogen intermediates from a single urea molecule remain on the adjacent sites throughout their multielectron oxidation until dinitrogen is formed and desorbed (Figure 2b). The advantage of the later mechanistic explanation is that it eliminates the need to consider a formation of three-membered cyclic intermediates-diaziridine-3-one and its reduced forms,[13b] which are rather strained and unstable structures.[19]

Since the N_2 formation mechanism requires adjacent sites for both N atoms in urea, while the one-nitrogen binding pathway that leads to $NO_x^- + NCO^-$ does not require the availability of adjacent sites on catalyst surface, the abundance of vacancies on the Ni sites should correlate with selectivity towards N_2 formation. Indeed, compared to the activated Ni foam, $Ni(OH)_2$ xerogel represents a very disordered structure and, therefore has more vacancies;[13c] this structural difference together with the two-times higher FE of N_2 obtained here on the xerogel compared to the activated Ni foam[13b] supports the proposed hypothesis. Further surface modifications to increase the number of defects such as stabilizing the α-$Ni(OH)_2$/γ-NiOOH phase could lead to increased N_2 selectivity.[13d]

We note that alternative mechanisms to the ones shown in Figure 2 should still be considered, especially for the formation of minor products, such as N_2O and CO (FE $<1\%$), which is not accounted for in the proposed pathways. Since N_2O (N oxidation state: $+1$) represents an over-oxidized product, we expect it to be formed in the later stages of the mechanisms shown in Figure 2. To understand whether N_2O and CO can be formed from the decomposition of cyanate, we performed a series of electrolyses of 0.33 M cyanate in 1 M KOH at 1.5 V, 1.7 V and 1.9 V with analysis of the reaction headspace using in-line GC-MS (Figure S7). In these experiments, the formation of trace amount of N_2O was observed at 1.7 V and 1.9 V, while CO was not detected at all studied potentials. These results show that N_2O can be formed through either urea or cyanate oxidation, indicating that similar N-containing intermediate is likely to be involved in both cases. While this work focuses on the formation mechanisms of major UOR products, further studies are required to elucidate the distinct formation mechanisms of minor products of UOR.

To further validate the major product formation mechanisms discussed above, we performed DFT calculations of energy barriers for the key steps of UOR to $NO_x^- + NCO^-$ and to $N_2 + CO_2$ (Figure 3, see Supporting Information for details, p. S14–S18). In these calculations, NiOOH surfaces containing one or two vacancies were considered (Figures 3a, S15, and S16). Firstly, we found that the coordination of urea to the catalyst surface is more favourable for the surface with more vacancies (Figures 3b,c, and Table S4), which explains higher UOR activity (current densities) observed on disordered materials.[13c,20] In terms of the pathway selectivity, DFT revealed that when the surface has adjacent vacancies, the cleavage of N–C bond is less favourable (Figure 3b). In contrast, when the surface lacks adjacent vacancies, it is more energetically favourable for the $*NHCONH_2$ intermediate to undergo the C–N cleavage rather than further deprotonation to *NHCONH (Figure 3c). Thus, the DFT data supports that the lack of vacancies favours N–C cleavage and, therefore, favours the $NO_x^- + NCO^-$ formation pathway, while the abundance of vacancies suppresses N–C cleavage, favouring $N_2 + CO_2$ formation pathway.

Based on the obtained mechanistic insights, we hypothesized that doping of NiOOH with a secondary metal could alter the ability of urea to coordinate and undergo oxidation via one- vs two-nitrogen pathways. In previous works, it has been shown that even a small amount of a dopant can alter the electronic structure of the surrounding Ni sites and, as a result, change its electrochemical behaviour.[11d] To test the

© 2022 Wiley-VCH GmbH

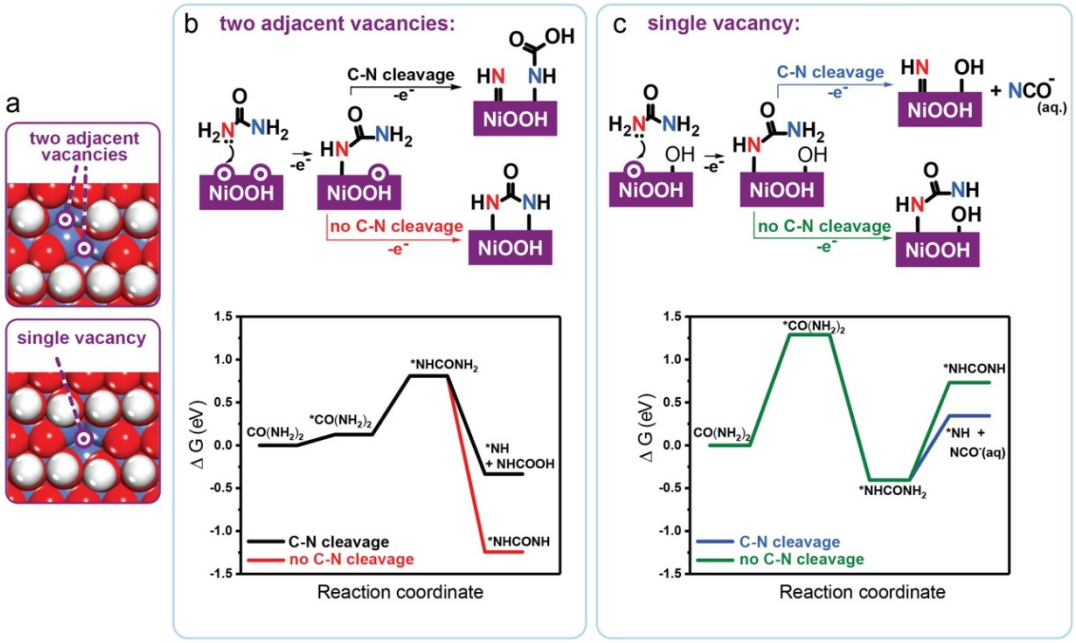

Figure 3. Comparison of energetic availability of C–N cleavage (leading to NCO^- formation) and no C–N cleavage pathways on NiOOH with one and two adjacent vacancies on Ni sites using DFT. a) The atomic structures of the NiOOH surface with two adjacent vacancies (top) and one vacancy (bottom); navy balls correspond to Ni, "red" to O, and "white" to H atoms (see Figures S15–S16 for further details). b,c) A schematic illustration (top) and free energy diagram (bottom) of the possible intermediates in the key steps of UOR proceeding on the surface with two adjacent vacancies on Ni in NiOOH (b) or a single vacancy (c).

doping influence on the UOR product selectivity, we chose a low (20 %) dopant loading and tested $Ni(OH)_2$ doped with each of the three earth-abundant and inexpensive metals: Co, Fe, and Cu.

While doping $Ni(OH)_2$ with Co or Fe showed improvement of the UOR onset potential in agreement with previous reports,[11d,21] we found that neither Co nor Fe improved the reaction selectivity towards N_2 compared to that of $Ni(OH)_2$ (Figure S8a,b). In contrast to Co and Fe, the introduction of 20 % of Cu (Figures 4a, b; for material characterization see Figures S9–S13) almost doubled the N_2 selectivity (55 % FE of N_2 at 1.4 V) compared to the undoped $Ni(OH)_2$ (FE of N_2 up to 30 %). Interestingly, the FE of N_2 remained around 50 % even at more positive potentials (1.5 V and 1.6 V), while a significant decrease was observed for the undoped $Ni(OH)_2$ catalyst at these potentials (Figure 1b). A long-term potentiostatic UOR electrolysis at 1.6 V over 48 h using $Ni_{0.8}Cu_{0.2}(OH)_2$ demonstrated that the suppression of urea overoxidation on Cu-doped $Ni(OH)_2$ remains high compared to an undoped

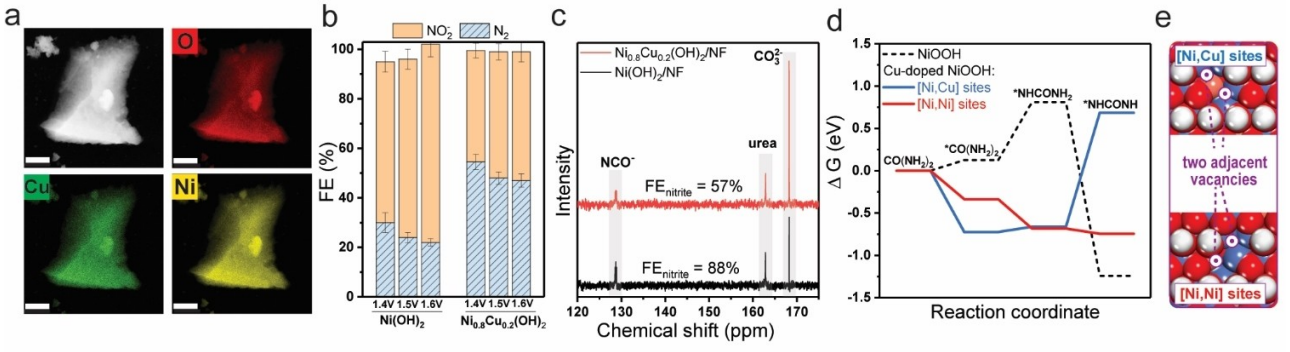

Figure 4. a) Dark field TEM and elemental composition of $Ni_{0.8}Cu_{0.2}(OH)_2$ determined using EDX mapping. Scale bars, 500 nm. b) FEs of the major products of short-term urea electrolysis at $Ni(OH)_2$/NF, $Ni_{0.8}Cu_{0.2}(OH)_2$/NF, and PANI-$Ni_{0.8}Cu_{0.2}(OH)_2$/NF anodes at 1.4–1.6 V. c) NMR spectra recorded for long-term UOR on $Ni(OH)_2$/NF (black trace) and $Ni_{0.8}Cu_{0.2}(OH)_2$/NF (red trace) anodes. d) Free energy diagrams for the possible key steps of UOR to N_2 on the Cu-doped NiOOH surface with two adjacent vacancies. e) The structures show the surface of Cu-doped NiOOH with two adjacent vacancies (navy balls correspond to Ni, "orange" to Cu, "red" to O, and "white" to H atoms).

© 2022 Wiley-VCH GmbH

catalyst over a long period of time (FEs of nitrite were 57 and 88 % on doped and undoped $Ni(OH)_2$, respectively; Figure 4c). In addition, we found that in the case of $Ni_{0.8}Cu_{0.2}(OH)_2$ the reaction mixture contains less cyanate and more carbonate compared to $Ni(OH)_2$-catalyzed UOR (Figure 4c). This observation further supports that carbonate originates from the N_2 pathway, while cyanate is formed through NO_x^- pathway.

To better understand why Cu doping improves the catalyst selectivity towards N_2, we performed DFT calculations of energy barriers for the key steps of the UOR to N_2 pathway, which proceeds through the coordination of both N atoms in urea molecule to two adjacent catalytic sites (Figure 3a,c). In the case of Cu-doped NiOOH, these catalytic sites can either involve Cu ([Ni, Cu] sites) or not ([Ni, Ni] sites), as shown in Figure 4d (see Supporting Information for details, p. S14–S17, Figures S17 and S18). We found that in both cases the introduction of Cu noticeably decreases the energy requirements for urea adsorption and the following oxidation to $*NHCONH_2$ compared to undoped $Ni(OH)_2$. Further oxidation of this intermediate to *NHCONH is more energetically favoured when it is bound to [Ni, Ni] sites compared to when it is bound to [Ni, Cu] sites, due to the weak coordination of N to Cu. The results of calculations indicate that the main role of Cu doping is altering the electronic structure of the surrounding Ni sites and thereby lowering the energies of key intermediates, rather than acting as an active site itself.

Recently, Li et al.[13b] demonstrated another way to improve N_2 selectivity in UOR: polyaniline (PANI) overcoating of activated NF allowed to increase N_2 FE by 15 % compared to bare NF. The authors attributed the selectivity improvement to PANI creating a hydrogen-bonding network on the electrode surface, which increased the residence time of urea molecules near the active sites, thereby improving the catalyst performance towards the formation of N_2.[13b] When we combined this approach with Cu-doping, N_2 selectivity increased further from 55 % to 65 %, making N_2 the major reaction product (Figure S8c). While the role of polymer coatings on the UOR selectivity of Ni-based catalysts needs to be further investigated mechanistically, this result demonstrated that different catalyst design strategies can be successfully combined to boost N_2 selectivity in UOR.

Conclusion

In summary, we showed that urea electrolysis in alkaline media at $Ni(OH)_2$ anodes predominantly leads to the formation of near-stoichiometric ratio of NO_x^- and cyanate (NCO^-) in a wide range of potentials (FE of NO_x^- is up to 88 %), while carbonate is formed through the less favourable N_2 formation pathway. Based on the experimental data and DFT calculations, we proposed a comprehensive mechanistic model disambiguating the reaction paths to these products, which suggests a strong influence of the active site availability and their electronic structure on the selectivity of UOR. Specifically, cyanate (and concomitant NO_x^-) formation proceeds through the nitrogen-carbon bond cleavage in urea, which is more favourable when urea coordination to the surface via both N atoms is hindered. We found that by increasing the availability of active sites on the catalyst (by using disordered $Ni(OH)_2$ xerogel) or making binding of the second N atom more energetically accessible (by introducing Cu doping that alters the electronic structure of Ni sites) the cleavage of nitrogen-carbon bond and formation of overoxidation products can be suppressed, while binding of urea via two N atoms becomes promoted, resulting in higher selectivity towards N_2 formation. Thus, using $Ni_{0.8}Cu_{0.2}(OH)_2$ xerogel boosted the FE of N_2 to above 50 %. The reported mechanistic insights are foundational for the further development of active and selective UOR catalysts and achieving a complete suppression of urea overoxidation.

Acknowledgements

The authors thank Dr. Brian Kendall for his help with ICP-MS characterization. The authors acknowledge the financial support from the University of Waterloo, Waterloo Institute for Nanotechnology, Agriculture and Agri-Food Canada (Agricultural Clean Technology Program), Natural Sciences and Engineering Council of Canada (DG and RTI Funds), Canada Foundation for innovation, and Ontario Research Fund.

Conflict of Interest

The authors declare no conflict of interest.

Data Availability Statement

The data that support the findings of this study are available in the supplementary material of this article.

Keywords: Electrocatalysis · Nickel · Overoxidation · Reaction Mechanism · Urea Electrolysis

[1] a) J. H. Meessen, *Urea. In Ullmann's Encycl. Ind. Chem.*, Wiley-VCH, Weinheim, **2000**; b) B. M. Comer, P. Fuentes, C. O. Dimkpa, Y.-H. Liu, C. A. Fernandez, P. Arora, M. Realff, U. Singh, M. C. Hatzell, A. J. Medford, *Joule* **2019**, *3*, 1578–1605.
[2] L. Celleno, *Dermatol. Ther.* **2018**, *31*, e12690.
[3] M. Koebel, M. Elsender, M. Kleemann, *Catal. Today* **2000**, *59*, 335–345.
[4] E. Urbańczyk, M. Sowa, W. Simka, *J. Appl. Electrochem.* **2016**, *46*, 1011–1029.
[5] L. E. Scherger, V. Zanello, C. Lexow, *Bull. Environ. Contam. Toxicol.* **2021**, *107*, 565–573.
[6] W. H. R. Shaw, J. J. Bordeaux, *J. Am. Chem. Soc.* **1955**, *77*, 4729–4733.

© 2022 Wiley-VCH GmbH

[7] L. E. Krausfeldt, A. T. Farmer, H. F. C. Gonzalez, B. N. Zepernick, S. R. Campagna, S. W. Wilhelm, *Front. Microbiol.* **2019**, *10*, 1064.
[8] P. M. Glibert, J. Harrison, C. Heil, S. Seitzinger, *Biogeochemistry* **2006**, *77*, 441–463.
[9] a) B. Zhu, Z. Liang, R. Zou, *Small* **2020**, *16*, 1906133; b) R. K. Singh, K. Rajavelu, M. Montag, A. Schechter, *Energy Technol.* **2021**, *9*, 2100017; c) K. Ye, G. Wang, D. Cao, G. Wang, *Top. Curr. Chem.* **2018**, *376*, 42; d) W. Xu, Z. Wu, S. Tao, *Energy Technol.* **2016**, *4*, 1329–1337.
[10] a) X. V. Medvedeva, J. J. Medvedev, S. W. Tatarchuk, R. M. Choueiri, A. Klinkova, *Green Chem.* **2020**, *22*, 4456–4462; b) X. V. Medvedeva, J. J. Medvedev, A. Klinkova, *Adv. Energy Sustainability Res.* **2021**, *2*, 2100001; c) L. Wang, Y. Zhu, Y. Wen, S. Li, C. Cui, F. Ni, Y. Liu, H. Lin, Y. Li, H. Peng, B. Zhang, *Angew. Chem. Int. Ed.* **2021**, *60*, 10577–10582; *Angew. Chem.* **2021**, *133*, 10671–10676.
[11] a) Y. Wang, C. Wang, H. Shang, M. Yuan, Z. Wu, J. Li, Y. Du, *J. Colloid Interface Sci.* **2022**, *605*, 779–789; b) X. Li, X. Cui, L. Jiang, *Catal. Commun.* **2022**, *162*, 106390; c) H. Wang, X. Jiao, W. Zheng, Y. Zhang, Y. Jiao, *Int. J. Hydrogen Energy* **2021**, *46*, 37792–37801; d) S. W. Tatarchuk, R. M. Choueiri, X. V. Medvedeva, L. D. Chen, A. Klinkova, *Chemosphere* **2021**, *279*, 130550.
[12] a) V. T. Veettil, A. U. Vijayakumar, A. Ashdot, D. Zitoun, *ACS Appl. Energy Mater.* **2022**, *5*, 1397–1402; b) J. Wang, Y. Sun, Y. Qi, C. Wang, *ACS Appl. Mater. Interfaces* **2021**, *13*, 57392–57402; c) Q. Zhao, C. Meng, D. Kong, W. Wang, H. Hu, X. Chen, Y. Han, X. Chen, Y. Zhou, M. Lin, M. Wu, *ACS Sustainable Chem. Eng.* **2021**, *9*, 15582–15590.
[13] a) Q. He, Y. Wan, H. Jiang, Z. Pan, C. Wu, M. Wang, X. Wu, B. Ye, P. M. Ajayan, L. Song, *ACS Energy Lett.* **2018**, *3*, 1373–1380; b) J. Li, J. Li, T. Liu, L. Chen, Y. Li, H. Wang, X. Chen, M. Gong, Z.-P. Liu, X. Yang, *Angew. Chem. Int. Ed.* **2021**, *60*, 26656–26662; *Angew. Chem.* **2021**, *133*, 26860–26866; c) L. Zhang, L. Wang, H. Lin, Y. Liu, J. Ye, Y. Wen, A. Chen, L. Wang, F. Ni, Z. Zhou, S. Sun, Y. Li, B. Zhang, H. Peng, *Angew. Chem. Int. Ed.* **2019**, *58*, 16820–16825; *Angew. Chem.* **2019**, *131*, 16976–16981; d) S. Chakrabarty, I. Offen-Polak, T. Y. Burshtein, E. M. Farber, L. Kornblum, D. Eisenberg, *J. Solid State Electrochem.* **2021**, *25*, 159–171.
[14] a) B. K. Boggs, R. L. King, G. G. Botte, *Chem. Commun.* **2009**, 4859–4861; b) W. Yan, D. Wang, L. A. Diaz, G. G. Botte, *Electrochim. Acta* **2014**, *134*, 266–271; c) D. Wang, S. H. Vijapur, Y. Wang, G. G. Botte, *Int. J. Hydrogen Energy* **2017**, *42*, 3987–3993.
[15] J. J. Medvedev, Y. Tobolovskaya, X. V. Medvedeva, S. W. Tatarchuk, F. Li, A. Klinkova, *Green Chem.* **2022**, *24*, 1578–1589.
[16] Y. Koyama, Y.-G. Lee, S. Kuroki, T. Takata, *Tetrahedron Lett.* **2015**, *56*, 7038–7042.
[17] R. M. Choueiri, S. W. Tatarchuk, A. Klinkova, L. D. Chen, *Electrochem. Sci. Adv.* **2021**, https://doi.org/10.1002/elsa.202100142.
[18] W. Chen, L. Xu, X. Zhu, Y.-C. Huang, W. Zhou, D. Wang, Y. Zhou, S. Du, Q. Li, C. Xie, L. Tao, C.-L. Dong, J. Liu, Y. Wang, R. Chen, H. Su, C. Chen, Y. Zou, Y. Li, Q. Liu, S. Wang, *Angew. Chem. Int. Ed.* **2021**, *60*, 7297–7307; *Angew. Chem.* **2021**, *133*, 7373–7383.
[19] a) J. F. Liebman, A. Greenberg, *J. Org. Chem.* **1974**, *39*, 123–130; b) F. D. Greene, J. C. Stowell, W. R. Bergmark, *J. Org. Chem.* **1969**, *34*, 2254–2262; c) F. D. Greene, J. F. Pazos, *J. Org. Chem.* **1969**, *34*, 2269–2274.
[20] a) Q. Zhang, M. Sun, J. Zhu, S. Yang, L. Chen, X. Yang, P. Wang, K. Li, F. Xue, Y. Lu, J. Zhang, P. Zhao, *Chem. Eng. J.* **2022**, *432*, 134275; b) S. Zheng, Y. Zheng, H. Xue, H. Pang, *Chem. Eng. J.* **2020**, *395*, 125166.
[21] X. Yang, H. Zhang, B. Yu, Y. Liu, W. Xu, Z. Wu, *Energy Technol.* **2022**, *10*, 2101010.

Manuscript received: July 5, 2022
Accepted manuscript online: August 5, 2022
Version of record online: ■■, ■■

© 2022 Wiley-VCH GmbH

Research Articles

Electrocatalysis

S. W. Tatarchuk, J. J. Medvedev, F. Li, Y. Tobolovskaya, A. Klinkova* _____ **e202209839**

Nickel-Catalyzed Urea Electrolysis: From Nitrite and Cyanate as Major Products to Nitrogen Evolution

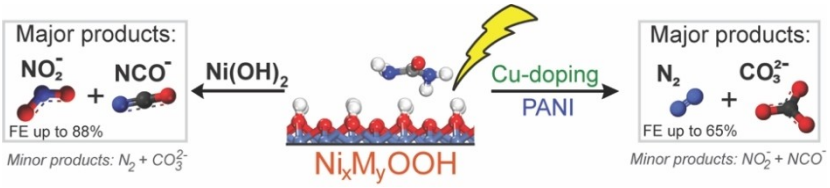

Urea electrooxidation to N_2 is a promising anodic process for producing renewable fuels at the cathode. However, Ni(OH)$_2$-catalyzed urea oxidation predominantly produces a ≈1:1 mixture of nitrite + cyanate, with N_2 being a minor product. A mechanistic analysis suggests that the binding site availability for both N atoms in urea is crucial for reaction selectivity. Doping Ni(OH)$_2$ with Cu significantly suppresses the cyanate + nitrate pathway.

© 2022 Wiley-VCH GmbH